Nanostructures

Deutsche Ausgabe: DOI: 10.1002/ange.201411460
Internationale Ausgabe: DOI: 10.1002/anie.201411460

Metal Redox Processes for the Controlled Synthesis of Metal Alloy Nanoparticles**

*Alec Kirkeminde, Stan Spurlin, Laura Draxler-Sixta, Jamie Cooper, and Shenqiang Ren**

Abstract: *Nanocrystalline metals have received widespread interest and found various applications owing to their magnetic and catalytic properties and in energy-related fields. A flexible approach for the growth of nanoalloys with controlled properties and well-defined structures on the atomic scale is thus greatly desired. A new synthetic method that avoids incompatible reduction potentials and rates would be critical to grow metal nanostructures with high purities and the desired stoichiometries. A metal-redox strategy that employs spontaneous oxidation/reduction reactions to grow nanocrystalline alloys using molecular-scale zerovalent metal precursors is now described. The selection of suitable zerovalent metal species allows for thermodynamic control of the compositional stoichiometry during the temperature-dependent formation of the metal alloy nanoparticles. A practical and scalable strategy for nanoalloy growth that can potentially produce key metal components of superior metallurgical quality for catalytic and magnetic systems has thus been developed.*

The remarkable interest in nanocrystalline metals and alloys has been invoked by their high surface area to volume ratio, excellent strength, and unique nanostructures.[1] Many types of metal alloy nanoparticles have been explored in the past owing to their interesting practical applications, for example, as nanocatalysts and high-energy nanomagnets.[2] Therefore, different top-down and bottom-up methods for synthesizing metal alloy nanoparticles have been intensively studied, such as ball milling, electrodeposition, and solution-phase synthesis, with the latter seeing rapid growth owing to the simplicity of scaling up and the economical setup.[3] Bottom-up solution-processing methods utilize three main components: metal precursors (predominantly metal salts), reducing agents, and organic ligands.[4] In general, the reduction potentials of the metal ions dictate the selection of the reducing agents, adding to the complexity of the process.[5] Moreover, when it comes to alloying bi- or trimetallic compounds, reduction rates become an issue that must be considered to allow for proper alloying. Organic ligands are thought to be necessary owing to the shape and size control they provide to the metal nanoparticle, but pose a dilemma after the synthesis as they still passivate the exposed surface planes, coordinate to active sites, and add excess mass to or even dope the final systems.[2i,6] Various studies have been conducted on how to remove these coordinated ligands with varying success.[6,7] To avoid these obstacles, a synthetic method that does not suffer from these drawbacks, while still producing nanostructured alloys, is needed. It is known that a zerovalent metal itself has an inherent reducing ability. However, to the best of our knowledge, this electrochemical energy has not be used to synthesize and control nanostructured alloys thus far. Using electrochemical redox reactions, a highly versatile and straightforward metal-redox method for the ligand-free synthesis of metal alloy nanoparticles is presented in this study.

According to this strategy, three reagents are required for generic binary M_aM_b nanoalloys: a solvent, a zerovalent M_a metal source, and an M_b metal salt. Scheme 1 presents a basic outline of the metal redox process. In part a, both metal species are in their original states, one as a zerovalent species (M_a^0) and the other one in its oxidized form (M_b^{n+}). After reduction of the metal M_b^{n+} salt with the zerovalent M_a^0 precursor (part b), the metals can then be alloyed to obtain the final M_aM_b nanoalloy (part c). For metal salts, simple metal acetylacetonate (acac) complexes were used as the metal salts whereas $[Fe(CO)_5]$, $[Co_2(CO)_8]$, $[Mn_2(CO)_{10}]$, and $[Ni(cod)_2]$ (cod = cyclooctadiene) were used as the zerovalent metal precursors in this study. A generic set of reactions elucidates whether the metal-redox process can be employed:

$$2\,M_a^0 \rightleftharpoons M_a^{n+} + M_a^0 + n\,e^- \quad E^\circ = x \tag{1}$$

$$M_b^{n+} + n\,e^- \rightleftharpoons M_b^0 \quad E^\circ = y \tag{2}$$

$$2\,M_a^0 + M_b^{n+} \rightleftharpoons M_a M_b + M_a^{n+} \tag{3}$$

If $E_{cell} = (x + y) > 0$, the reaction will proceed.

For example, taking the half-reaction values for Fe^0 and Ni^{2+} ($x = +0.44$ V and $y = -0.25$ V, respectively) gives a value for E_{cell} of $+0.19$ V, which dictates that this reaction will be spontaneous. Even though values determined under standard conditions were used to obtain this value, the reaction still occurs even with ligands coordinated to the metal cations or at high temperatures. It is important to note that these reactions are all in equilibrium and do not go to completion, allowing any unreacted M^0 species to alloy, producing the final bimetallic nanoparticles. Overall, when Fe^0 species are utilized as the zerovalent source, any metal cation with a reduction potential greater than -0.44 V can be used,

[*] A. Kirkeminde, S. Spurlin, L. Draxler-Sixta, J. Cooper, Prof. S. Ren
Department of Chemistry, University of Kansas
Lawrence, KS 66045 (USA)
E-mail: shenqiang@ku.edu

[**] S.R. is grateful for financial support from the National Science Foundation (NSF-CMMI-1332658). A.K. would like to thank the Microscopy and Analytical Imaging (MAI) laboratory at KU for help with TEM characterization and Dr. Victor Day for help with XRD characterization.

Supporting information for this article is available on the WWW under http://dx.doi.org/10.1002/anie.201411460.

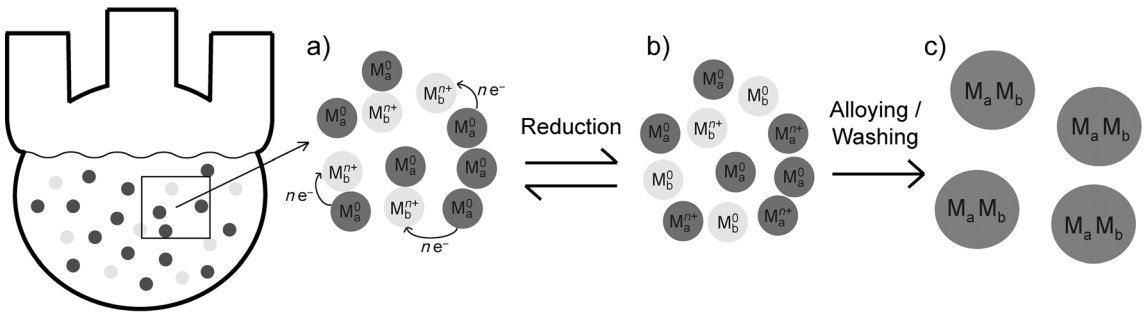

Scheme 1. a) Of the two metal precursors, one is present in its zerovalent state and the other one in an oxidized state. b) After reduction of the oxidized species, a mixture of both metals in their zerovalent states is present, which can then form the final nanoalloys (c).

meaning that Co^{2+} ($E° = -0.21$ V), Pd^{2+} ($E° = 0.915$ V), and Pt^{2+} ($E° = 1.188$ V) are all suitable choices. Taking this into consideration, Figure 1 displays a vast array of different metal nanoalloys that can be synthesized by simply using different zerovalent metal sources and metal salt precursors. As a concrete example, with the metal-redox strategy, the chemical synthesis of unique magnetically hard MnBi particles was achieved for the first time (Figure 1k), which has been a challenge owing to the vast difference between the reduction potentials of metallic Mn and Bi. Complete synthetic procedures and characterizations, including X-ray diffraction and magnetic data for all of the nanoalloys along with a table of $E°$ values for the half reactions of various metals, are given in the Supporting Information (Figure S1, S2 and Table S1).

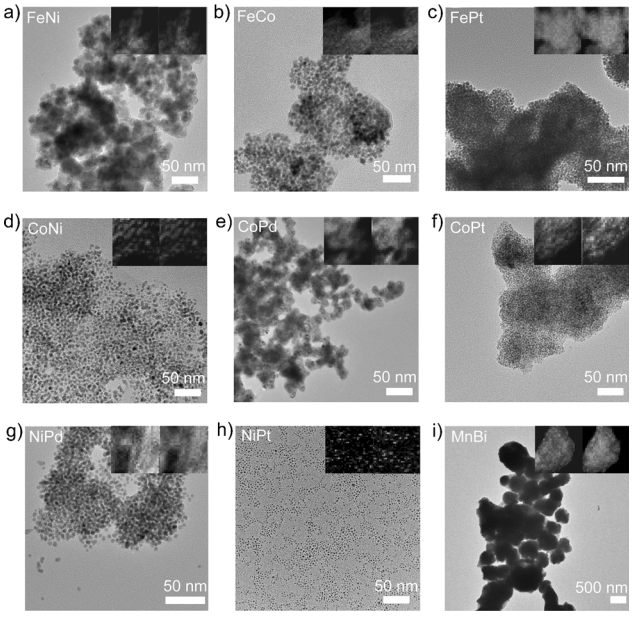

Figure 1. a–c) Particles obtained with $[Fe(CO)_5]$ as the zerovalent metal source. d–e) Particles obtained with $[Co_2(CO)_{10}]$ as the zerovalent metal source. g, h) Nanoalloys obtained with $[Ni(cod)_2]$ as the zerovalent metal source. i) MnBi particles obtained with $[Mn_2(CO)_{10}]$ as the zerovalent metal source. Acetylacetonate complexes were used for the oxidized metal sources except for bismuth, where bismuth neodecanoate was used.

Binary FeNi and ternary FeNiPd systems were utilized to demonstrate the flexibility of this metal-redox strategy. As these metal redox reactions are in equilibrium, both the reaction temperature and the precursor loading control the stoichiometry of the final nanoalloy particles. To demonstrate these effects, binary FeNi alloys with Ni/Fe molar loading ratios of both 1:2 and 1:1 were synthesized at different reaction temperatures. The reaction temperature dependence of the Ni/Fe ratios in the final product starting from either a 1:2 or a 1:1 ratio is displayed in Figure 2. All ratios were determined by energy-dispersive X-ray spectroscopy (EDS) and confirmed with inductively coupled plasma atomic emission spectroscopy (ICP-AES) and absorption measurements (Figure S3, S4). In both cases, the particles exhibit a higher Ni content when annealed at lower temperatures than at higher temperatures. This phenomenon can be rationalized by considering a simple chemical equilibrium: $Fe^0 + [Ni(acac)_2] \rightleftharpoons Ni^0 + [Fe(acac)_2]$. As discussed above, this reaction is spontaneous as $E_{cell} > 0$, but does not go to completion, allowing for zerovalent species of both metals to alloy. It is known that a lower temperature favors the forward reaction, leading to a higher nickel content. When the thermal energy is increased, the reverse reaction or non-spontaneous reaction becomes more favorable, which leads to alloys with a higher Fe content. At 548 K and 573 K, the compositions of the final products stagnate at the precursor loading amounts for both original ratios. It seems that the reaction can only be pushed to a ratio of 1, producing a stoichiometry equal to the molar loading amount, as all other binary reactions carried out at 573 K have produced compositions that match the precursor amount added (Table S2). A pseudo-equilibrium constant can be determined for this reaction, $K = [Ni^0]/[Fe^0]$, when the metal precursors are used in a ratio of 1:1. When larger amounts of Fe^0 are used (e.g., Ni/Fe = 1:2), the equation for K must be changed accordingly as the excess amount of Fe^0 in the alloy must be taken into account. The pseudo-equilibrium constants determined for the syntheses of various NiFe alloy nanoparticles are given in Figure 2b. By determining the K values of reactions carried out at different temperatures, we can then utilize $\ln(K) = -(\Delta H/R)(1/T) + \Delta S/R$ to create a Van't Hoff plot (Figure 2c) where ΔH and ΔS are the enthalpy and entropy changes, R is the gas constant, and T is the reaction temperature. Determining the equation of the fitted line allows the enthalpy of the reaction to be calculated. Solving for ΔH yields a value of -19.9 kJ mol^{-1} for

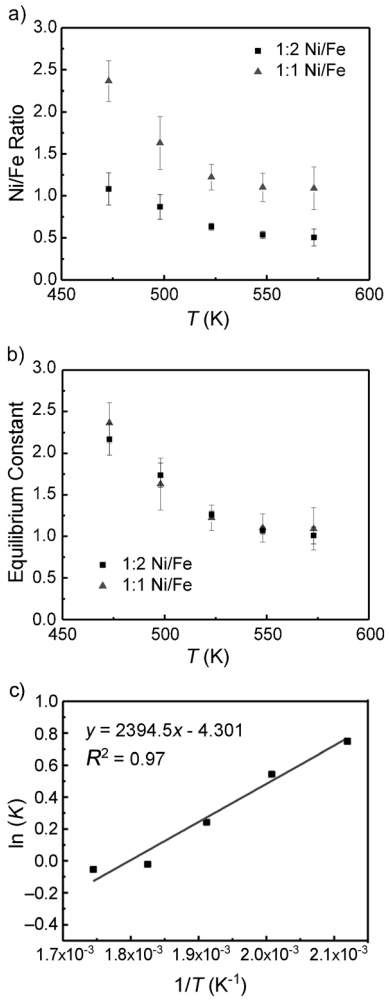

Figure 2. a) EDS data showing the stoichiometry of the final particles obtained using initial Ni/Fe ratios of either 1:2 or 1:1. b) Pseudo-equilibrium constant determined for the reaction of $[Fe(CO)_5]$ and $[Ni(acac)_2]$. c) Van't Hoff plot and linear fit.

FeNi. More importantly, the equation allows for the simple determination of the equilibrium constant at different reaction temperatures, which is directly related to the stoichiometry of the final nanoalloy. It should be noted that the K value is independent of the precursor loading and can be shifted by the reaction temperature, which allows for the control of the Ni/Fe ratio in the final particles by adjusting the temperature and the amount of zerovalent metal precursor M_a. All other alloy nanoparticles presented in this work can be studied in a similar fashion, as the reactions are all controlled by chemical equilibria.

Moreover, ternary nanostructured alloys can be made as long as the reduction potential of the zerovalent metal precursor is strong enough to reduce the metal salts used. Ternary FeNiPd nanoalloy systems with Fe/Ni/Pd molar ratios of $2{:}x{:}y$ $(x+y=1)$ were investigated. A reaction temperature of 573 K was used to ensure $K \approx 1$ (see above) to readily control the final stoichiometry. To examine the effects of different Pd and Ni loadings, we synthesized various nanoalloy systems with x and y values ranging from 0 to 1. XRD patterns of these different samples and their stoichiometries are given in Figure 3a. Increasing the Ni concentration within the ternary FePdNi system shifts the diffraction peak towards the FeNi phase, as the lattice is distorted by the introduction of more Ni atoms. Figure 3b shows a TEM image of $Fe_2Pd_{0.5}Ni_{0.5}$ and the EDS elemental maps. The magnetic characteristics of the particles with different stoichiometries are displayed in Figure 3c. The ordered FePd phase exhibited the highest coercivity (H_c) of the synthesized nanoalloy

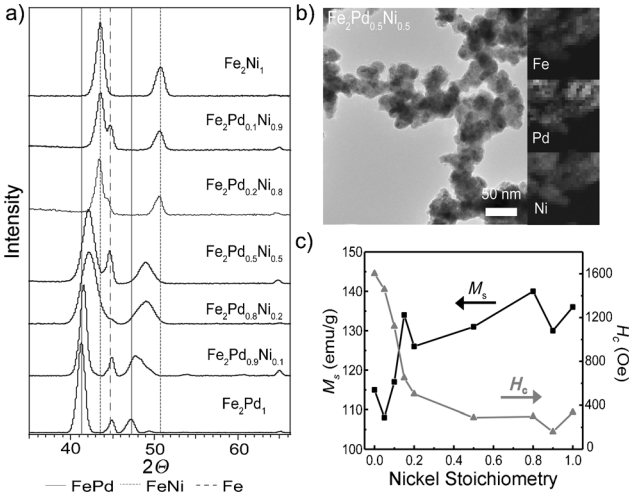

Figure 3. a) XRD patterns of FePdNi as the stoichiometry of the particles changes from Fe_2Pd to Fe_2Ni. b) TEM image and elemental mapping of $Fe_2Pd_{0.5}Ni_{0.5}$. d) Stoichiometry-dependent magnetic properties of the ternary FePdNi alloys.

particles.[2f,8] With a nickel dopant concentration of 15 wt%, the coercivity decreases drastically, which is in line with the ternary FePdNi phase diagram.[9] Above a nickel dopant concentration of approximately 15%, it significantly reduces the ordering parameter, whereas below this critical concentration, the system can consist of a mixture of ordered and disordered phases. An α-Fe phase was apparent in all ternary alloys, but not in the binary FeNi alloy. This is due to the thermodynamic stability of α-iron formation at an iron content of greater than 50% in the FePd phase diagram. Once the pure FeNi system has been reached, the α-iron peak disappears as an α-iron phase is not thermodynamically stable in a FeNi alloy.

We also studied the effects of this phase separation by looking at the catalytic activity of different ternary alloy systems. In particular, we selected the known catalytic reduction of *para*-nitrophenol to *para*-aminophenol with a large excess of sodium borohydride.[2m–n] This large excess allows for the assumption that the reaction rate is independent of the sodium borohydride concentration. The variations in the absorbance with time were measured for samples with various amounts of nickel and are displayed in Figure 4a. For a more in-depth investigation of the performance of the different particle systems, the turnover frequency (TOF) was calculated for each ternary system (Figure 4b). The largest TOF values were measured for the binary nanoalloy systems.

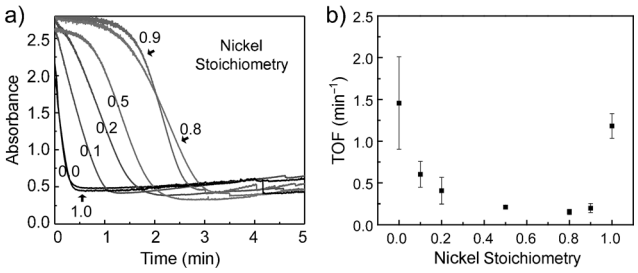

Figure 4. a) Absorption versus time spectra for ternary alloys with different stoichiometries. b) Calculated turnover frequencies for the particles with different stoichiometries.

We can attribute this lowering of the TOF values in the ternary nanoalloys to the presence of an α-iron phase. Compared to late transition metals, α-iron is relatively inert as a hydrogenation catalyst so that nanoalloy particles with an α-iron phase will have lower TOF values. The TOF value is thus higher in pure FeNi than in the ternary systems as there is no α-iron phase. In the case of pure FePd, as Pd is a superior catalyst, the highest TOF value was recorded for pure FePd despite the presence of an α-Fe phase. The metal nanocatalysts can be magnetically separated and recycled multiple times (Figure S5).

In conclusion, with our simple metal-redox method, a variety of bimetallic nanoalloy systems have been synthesized. Even more types of alloy systems may be obtained as long as the reduction potentials of the starting materials are compatible, making this a versatile method for the synthesis of nanoalloys that does not suffer from the use of different reducing agents or ligands. Using FeNi as an example, it was shown that the final stoichiometry of the particles can be easily controlled by adjusting the reaction temperature and explained with simple equilibrium concepts. Trimetallic alloy systems were also obtained in a controlled fashion, so that the magnetic and catalytic properties of the final particles can be easily tuned. These studies show that our metal-redox strategy can be universally utilized to produce many different nanocrystalline alloys for a variety of practical applications.

Experimental Section

1-Octadecene (ODE, 90%), toluene (ACS Grade), acetone (ACS Grade), $[Pd(acac)_2]$ (99%), $[Ni(acac)_2]$ (95%), $[Co(acac)_2]$ (97%), $[Pt(acac)_2]$ (97%), $[Fe(acac)_2]$ (97%), bismuth neodecanoate, $[Co_2(CO)_8]$ (>90% stabilized with hexanes), $[Fe(CO)_5]$ (99.99%), $[Mn_2(CO)_{10}]$ (98%), $[Ni(cod)_2]$, $NaBH_4$ (99%), *para*-nitrophenol (99.5%), nitric acid (>99.999%), and water (HPLC grade) were obtained from Sigma–Aldrich and used as received. For a standard Schlenk line synthesis, ODE (8 mL; degassed with argon) was added to a three-necked round-bottom flask, which was then evacuated and purged with argon and finally heated to the desired reaction temperature. Airtight vials were loaded with the selected precursors. For metal salts, they were filled with 0.25 mmol of the respective salt, and ODE (2 mL) was then added. Argon was bubbled through these solutions for 10 min, which were then heated on a stir plate at 352 K. For all zerovalent metal sources (aside from $[Fe(CO)_5]$, which was used as a neat liquid), the correct amount was added to another vial followed by 2 mL of ODE. The vial was degassed and set on a stir plate at 352 K. Once the desired temperature had been reached in the three-necked flask, the contents of both precursor vials were rapidly injected simultaneously and allowed to react for 1 hour. For the synthesis of MnBi particles, $[Mn_2(CO)_{10}]$ and bismuth neodecanoate were used in a 6:1 ratio as $[Mn_2(CO)_{10}]$ easily sublimes out of the solution. After the reaction, the particles were washed with a toluene/acetone mixture and centrifuged at 4000 rpm for 10 min. This procedure was repeated twice to remove any excess ODE and remaining metal salts. The sample was then moved to a nitrogen drybox where it was stored for further characterization. Samples were annealed at 773 K for 5 h in H_2/N_2 (1:9) atmosphere prior to magnetization and XRD measurements to increase their crystallinity and to remove any oxidation products formed during the workup. It is important to note that the pre-annealed NiPd and NiPt samples autoignite in air so care must be taken when handling these compounds.

Room-temperature X-ray powder patterns were obtained on a Bruker proteum diffraction system equipped with Helios multilayer optics, an APEX II CCD detector, and a Bruker MicroStar microfocus rotating-anode X-ray source operating at 45 kV and 60 mA. Transmission electron microscopy (TEM) images were obtained using a field-emission FEI Tecnai F20 XT. The magnetic hysteresis (M-H) loops were taken on a Microsense EZ7 vibrating sample magnetometer. A MTI GSL-1100X tube furnace was used for reductive sintering. Absorbance measurements were carried out with a Cary 100 Bio UV/Vis spectrophotometer.

The catalytic processes were analyzed according to previous reports.[2m–n] The catalyst (1 mg) was added to an aqueous *para*-nitrophenol solution (20 mL, 1.4×10^{-4} M), and the dispersion was briefly sonicated; then, sodium borohydride (32 mg, giving a 4.2×10^{-2} M solution) was added, and the mixture immediately transferred to a cuvette for absorbance measurements. The measurements were repeated five times for each sample. For recycling studies, the catalyst and the remaining reaction mixture were separated with the help of a strong magnet. The recovered catalyst was washed with water to remove any excess sodium borohydride or product. A new solution was then added, and the measurement repeated.

Keywords: alloys · magnetic properties · redox chemistry · stoichiometry

How to cite: *Angew. Chem. Int. Ed.* **2015**, *54*, 4203–4207
Angew. Chem. **2015**, *127*, 4277–4281

[1] a) B. Poudel, Q. Hao, Y. Ma, Y. Lan, A. Minnich, B. Yu, X. Yan, D. Wang, A. Muto, D. Vashaee, X. Chen, J. Liu, M. S. Dresselhaus, G. Chen, Z. Ren, *Science* **2008**, *320*, 634–638; b) L. Lu, Y. Shen, X. Chen, L. Qian, K. Lu, *Science* **2004**, *304*, 422–426; c) T. Chookajorn, H. A. Murdoch, C. A. Schuh, *Science* **2012**, *337*, 951–954; d) T. H. Fang, W. L. Li, N. R. Tao, K. Lu, *Science* **2011**, *331*, 1587–1590; e) K. Lu, *Science* **2014**, *345*, 1455–1456.

[2] a) H. Zeng, J. Li, Z. L. Wang, J. P. Liu, S. Sun, *Nano Lett.* **2003**, *4*, 187–190; b) H. Zeng, J. Li, J. P. Liu, Z. L. Wang, S. Sun, *Nature* **2002**, *420*, 395–398; c) Y. Yu, K. Sun, Y. Tian, X. Z. Li, M. J. Kramer, D. J. Sellmyer, J. E. Shield, S. Sun, *Nano Lett.* **2013**, *13*, 4975–4979; d) Y. Yu, W. Yang, X. Sun, W. Zhu, X. Z. Li, D. J. Sellmyer, S. Sun, *Nano Lett.* **2014**, *14*, 2778–2782; e) C. Wang, S. Peng, L.-M. Lacroix, S. Sun, *Nano Res.* **2009**, *2*, 380–385; f) T. Teranishi, A. Wachi, M. Kanehara, T. Shoji, N. Sakuma, M. Nakaya, *J. Am. Chem. Soc.* **2008**, *130*, 4210–4211; g) S. Sun, C. B. Murray, D. Weller, L. Folks, A. Moser, *Science* **2000**, *287*, 1989–1992; h) S. Sun, S. Anders, T. Thomson, J. E. E. Baglin, M. F. Toney, H. F. Hamann, C. B. Murray, B. D. Terris, *J. Phys. Chem. B* **2003**, *107*, 5419–5425; i) A. Kirkeminde, S. Ren, *Nano Lett.* **2014**, *14*, 4493–4498; j) M. Estrader, A. López-Ortega, S. Estradé, I. V. Golosovsky, G. Salazar-Alvarez, M. Vasilakaki, K. N. Trohidou, M. Varela, D. C. Stanley, M. Sinko, M. J. Pechan, D. J. Keavney, F. Peiró, S. Suriñach, M. D. Baró, J. Nogués, *Nat. Commun.* **2013**, *4*, 2960; k) C. Wang, H. Daimon, T. Onodera, T. Koda, S. Sun,

Angew. Chem. Int. Ed. **2008**, *47*, 3588 – 3591; *Angew. Chem.* **2008**, *120*, 3644 – 3647; l) W. Zhu, R. Michalsky, Ö. Metin, H. Lv, S. Guo, C. J. Wright, X. Sun, A. A. Peterson, S. Sun, *J. Am. Chem. Soc.* **2013**, *135*, 16833 – 16836; m) M. Schrinner, M. Ballauff, Y. Talmon, Y. Kauffmann, J. Thun, M. Möller, J. Breu, *Science* **2009**, *323*, 617 – 620; n) J. Zeng, Q. Zhang, J. Chen, Y. Xia, *Nano Lett.* **2009**, *10*, 30 – 35.

[3] a) L. Lu, M. L. Sui, K. Lu, *Science* **2000**, *287*, 1463 – 1466; b) M. Murayama, J. M. Howe, H. Hidaka, S. Takaki, *Science* **2002**, *295*, 2433 – 2435.

[4] a) A.-H. Lu, E. L. Salabas, F. Schüth, *Angew. Chem. Int. Ed.* **2007**, *46*, 1222 – 1244; *Angew. Chem.* **2007**, *119*, 1242 – 1266; b) R. Ghosh Chaudhuri, S. Paria, *Chem. Rev.* **2012**, *112*, 2373 – 2433; c) B. L. Cushing, V. L. Kolesnichenko, C. J. O'Connor, *Chem. Rev.* **2004**, *104*, 3893 – 3946.

[5] a) J. F. Bondi, K. D. Oyler, X. Ke, P. Schiffer, R. E. Schaak, *J. Am. Chem. Soc.* **2009**, *131*, 9144 – 9145; b) K. M. Hyie, I. I. Yaacob, *J. Mater. Process. Technol.* **2007**, *191*, 48 – 50; c) S. Sun, *Adv. Mater.* **2006**, *18*, 393 – 403.

[6] D. Li, C. Wang, D. Tripkovic, S. Sun, N. M. Markovic, V. R. Stamenkovic, *ACS Catal.* **2012**, *2*, 1358 – 1362.

[7] H. Zhang, B. Hu, L. Sun, R. Hovden, F. W. Wise, D. A. Muller, R. D. Robinson, *Nano Lett.* **2011**, *11*, 5356 – 5361.

[8] N. Sakuma, T. Ohshima, T. Shoji, Y. Suzuki, R. Sato, A. Wachi, A. Kato, Y. Kawai, A. Manabe, T. Teranishi, *ACS Nano* **2011**, *5*, 2806 – 2814.

[9] T. Horiuchi, M. Igarashi, F. Abe, K. Ohkubo, S. Miura, T. Mohri, *Metall. Mater. Trans. A* **2005**, *36*, 1999 – 2006.

Received: November 26, 2014
Published online: January 30, 2015

